Earth, Planets and Space

FULL PAPER

Open Access

Geomagnetic relative paleointensity and direction during the last 40,000 years obtained from a sediment core in the Nankai Trough

Ryoya Goto[1,2], Toshitsugu Yamazaki[1*], Natsumi Okutsu[1,3] and Juichiro Ashi[1]

Abstract

Construction of regional geomagnetic secular variation curves for the last several tens of thousands of years is important for understanding the behavior of non-dipole fields and applications to geochronology. Around Japan, secular variation records of older than 10 ka was scarce, in particular for relative paleointensity (RPI). Here, we conducted a paleomagnetic study of a sediment core covering the last ~ 40 kyr taken from a small basin in the Nankai Trough. The core consists of homogenous hemipelagic sediments except for turbidites and volcanic ashes. The age model was constructed based on seven ^{14}C datings and two volcanic ashes. Turbidites and volcanic ashes were excluded from the construction of secular variation curves because of geologically instantaneous deposition. It was revealed that the magnetization of this core is carried largely by detrital magnetic minerals, although magnetofossils are also contained. Bulk magnetic properties show some temporal changes in magnetic concentration and grain size, but still homogeneous enough for reliable RPI estimations except for turbidites and volcanic ashes. The resultant RPI shows no correlation with the normalizer, anhysteretic remanent magnetization, of the RPI estimations or with a proxy for a magnetic grain size and/or the proportion of magnetofossils to detrital magnetic minerals. The obtained RPI record shows a long-term increasing trend since ~ 40 ka, which coincides with global stack curves. On the other hand, there are some differences in shorter timescale variations, which may reflect non-dipole fields. This study demonstrated that hemipelagic sediments in the Nankai Trough have potential for recovering high-quality RPI records when turbidites and volcanic ashes were excluded and are useful for accumulating records to construct a regional master curve.

Keywords Relative paleointensity, Geomagnetic secular variation, Paleomagnetism, Rock magnetism, Nankai Trough

*Correspondence:
Toshitsugu Yamazaki
yamazaki@aori.u-tokyo.ac.jp
Full list of author information is available at the end of the article

Graphical abstract

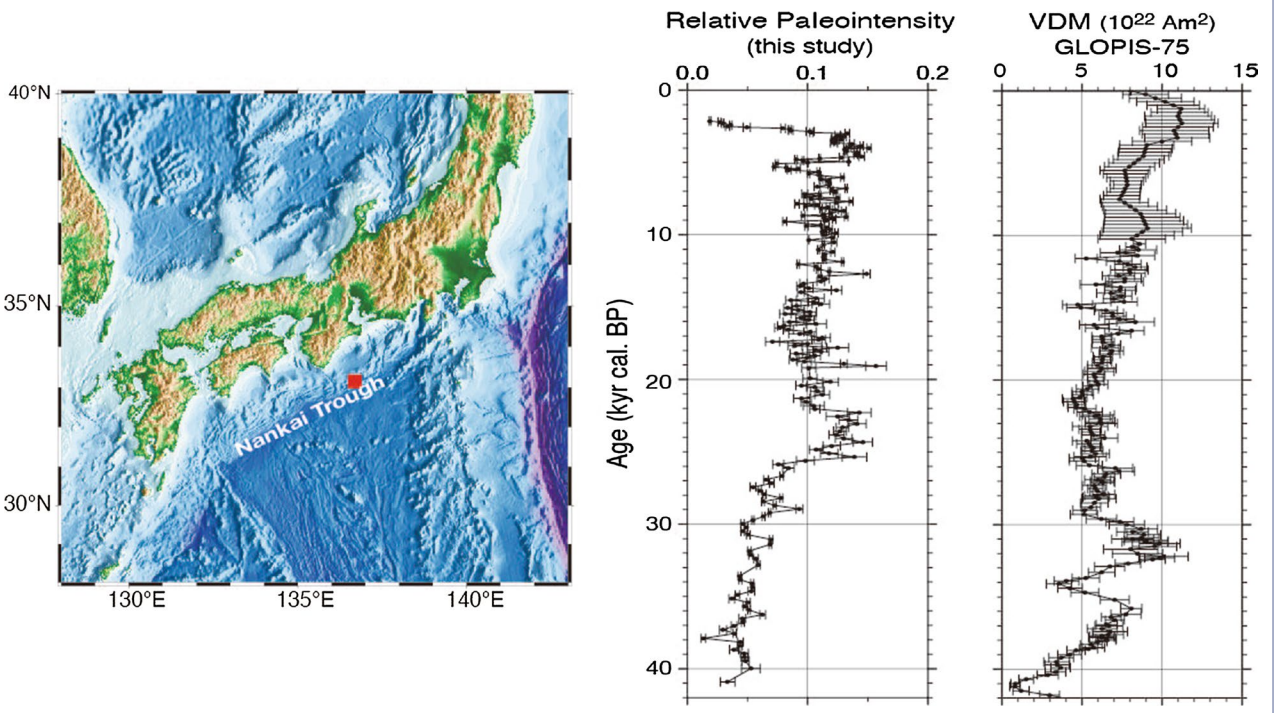

Main text

Introduction

Geomagnetic field variations have a very wide timescales from shorter than a second to millions of years or longer. Variations of longer than tens of years are considered to be originated from the Earth's interior, and knowledge of secular variations is important for understanding geodynamo processes in the core (Merrill et al. 1998). For the last 10 kyr, a large number of secular variation records were accumulated using archaeological materials, lake and marine sediments, and volcanic rocks, and global field models including non-dipole components were constructed (e.g., CALS10k, Korte et al. 2011). In addition to geomagnetic interests, regional reference curves of secular variations and predictions from global geomagnetic field models are useful also for geochronological applications, for example age estimations and inter-core correlations of sediment cores (Kanamatsu et al. 2017; Korte et al. 2019).

Efforts have been made to extend geomagnetic field models to older times, and a model for the last 100 ka was reported (GGF100k, Panovska et al. 2018). However, the spatial and temporal resolutions of this model is still limited because the number of available records is not enough for older than 10 ka and their site distribution is biased. Thus, further accumulation of regional paleomagnetic secular variation records of high enough resolutions is still necessary. For this purpose, sediments with high enough sedimentation rates are required. Around Japan, which is the target region of this paper, such sediments occur in forearc basins and landward trench slopes. Sediments in these depositional environments were previously imagined to be unsuitable for relative paleointensity (RPI) studies because magnetic properties including magnetic concentration, grain size, and mineralogy potentially have large fluctuations compared with pelagic sediments of slow deposition. Furthermore, in sediments of these regions, turbidites can frequently be intercalated. Turbidite layers need to be detected and excluded when time variations of the geomagnetic field are considered because these layers are of geologically instantaneous deposition. However, it was sometimes not easy to detect them when they are fine grained and difference in appearance compared with sediments below and above is subtle. The potential rock magnetic inhomogeneity and the presence of turbidite layers are probably the main reasons why sediments in forearc basins and landward trench slopes around Japan were seldom used for studies of secular variations, in particular of RPI. However, recent technological development including X-ray

CT scan and X-ray fluorescence (XRF) core scan for analyzing sediment cores have made it possible to efficiently identify and characterize turbidite layers (e.g., Rothwell et al. 2006; Van Daele et al. 2014; Okutsu et al. 2018; Hsiung et al. 2021).

In this paper, we present the results of a paleo- and rock magnetic study of a sediment core covering the last ~ 40 kyr, which was taken from the Nankai Trough. Geomagnetic secular variations older than 10 ka were little reported so far around Japan, in particular for variations in RPI. We show that the sediments have magnetic and sediment properties of homogeneous enough for reliable RPI estimations when turbidite and volcanic ash layers are excluded, and that reductive dissolution of magnetic minerals, which can be a problem in hemipelagic sediments with relatively large organic carbon inputs, has not occurred. Then, we present a RPI record as well as directional variations for the last 40 kyr.

Materials and age model

The sediment core PC04 used in this study was taken during R/V Hakuho-maru KH-17-2 cruise from the Nankai Trough (Fig. 1). The position and water depth of the coring site are 33° 15.19′′ N, 136° 39.22′′ E and 2255 m. The site is located at a small hill in an ENE–WSW elongated isolated basin between the accretionary prism and the forearc basin off Kumano. From the topographic features of the basin, it is expected that the basin does not receive sediment supply from the river–submarine canyon system and that it preserves most sedimentary records. Such a basin is called a terminal basin. We consider that the deposition in terminal basins is mostly continuous without significant hiatuses eroded by turbidites because turbidites in the depositional environment of terminal basins like the studied site are thought to be originated by surface sediment remobilization (Okutsu et al. 2018), which may not have capability of significant erosion.

The studied core consists mainly of hemipelagic mud and intercalates turbidites and volcanic ashes (Fig. 2). Sixteen fine-grained turbidite layers were identified based on visual core description, X-ray CT scan images, elemental profiles from an XRF core scanner, and physical properties including magnetic susceptibility (Okutsu et al. 2018; Okutsu 2019). Two volcanic ash layers are intercalated at 1.48–1.53 m and 4.19–4.24 m in depth, which are identified as the Kikai-Akahoya (K-Ah) ash (median age 7253 cal yr BP, Albert et al. 2019) and the Sambe-Ukinuno (SUk) ash (median age 19,551 cal yr BP, Albert et al. 2018), respectively (Okutsu 2019). These turbidite and volcanic ash layers were excluded in this study for the purpose of constructing a geomagnetic secular variation curve because they represent geologically infinitely short period of time.

To construct the age model of the core, dating with radiocarbon (^{14}C) was conducted using planktonic foraminifers extracted from seven horizons (Table 1 and Fig. 2). The measurements were carried out using a

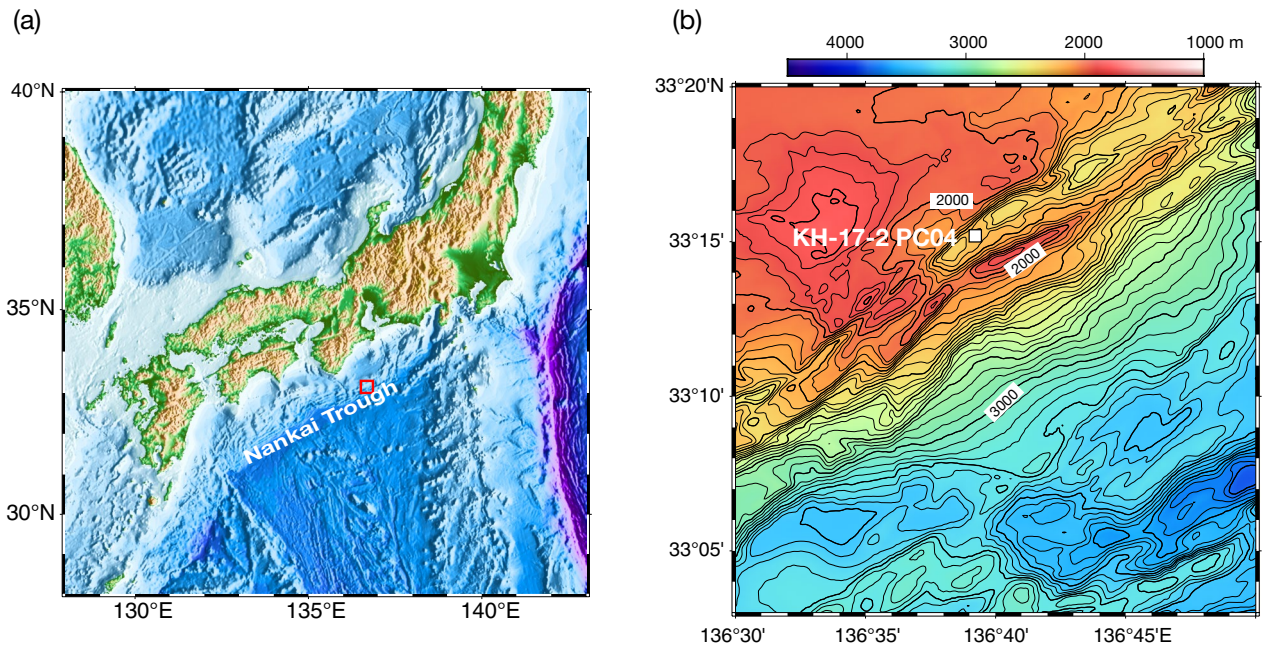

Fig. 1 **a** Shaded relief map of the Nankai Trough and surrounding areas. Red box indicates the area of panel **b**. **b** Topographic contour map in the vicinity of the site of Core KH-17–2 PC04. Contour intervals are 200 m (bold) and 50 m (thin)

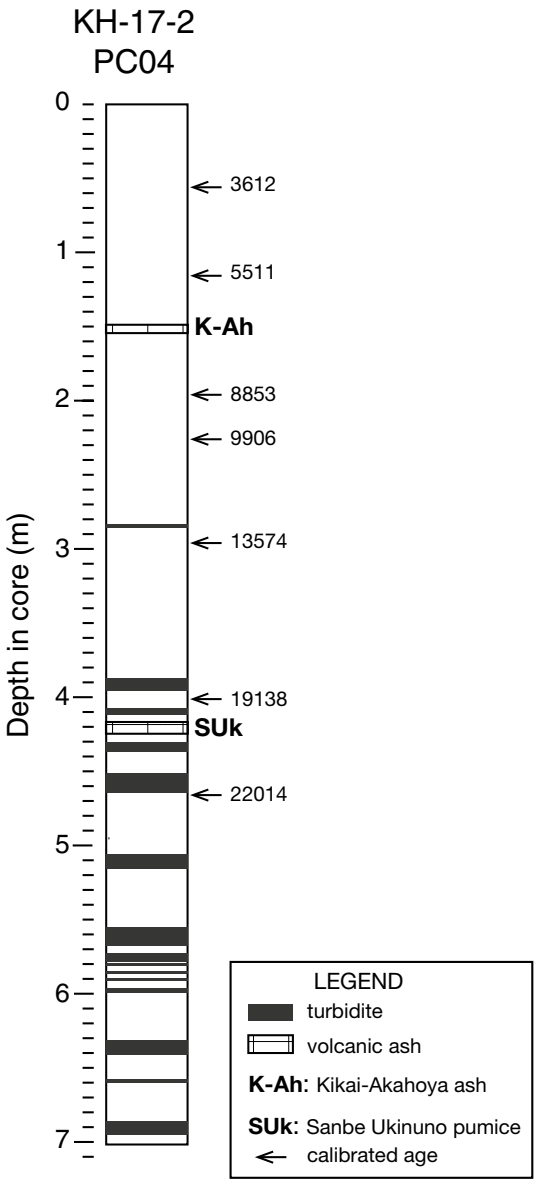

Fig. 2 Simplified columnar section of Core PC04. Median values of calendar ages are presented at the horizons where dating with ^{14}C was conducted

single-stage accelerator mass spectrometer at Atmosphere and Ocean Research Institute (AORI), The University of Tokyo. ^{14}C ages were converted to calendar ages based on the Marine20 calibration curve (Heaton et al. 2020) using the OxCal program version 4.4.2 (Bronk Ramsey 2009). We assumed zero year for the marine reservoir effect ($\Delta R = 0$). The median value of the calendar age was used to construct the age model shown in Fig. 3. The two ash layers mentioned above were also used as control points. Cumulative depth after excluding turbidite and ash layers were used as the depth scale in Fig. 3 and hereafter in this paper. Constant sedimentation rates were assumed between the dated horizons. Ages above (below) the uppermost (lowermost) dated horizon were extrapolated using the sedimentation rates of the adjacent dated intervals. The average sedimentation rate is approximately 18 cm/kyr, and the sedimentation rate increases upcore.

Discrete samples for rock- and paleomagnetic measurements were taken continuously from half-split core surface using 7 cc plastic cubes. In total 306 discrete samples were obtained.

Methods

Paleomagnetic direction and relative paleointensity

Natural remanent magnetization (NRM) was measured for all samples using a pass-through cryogenic magnetometer (2G Enterprises Model 760R) in a shielded room at Marine Core Research Institute (MaCRI), Kochi University. Stepwise alternating-field (AF) demagnetization of NRM was conducted at 15 steps, at 5 mT intervals up to 60 mT and at 70 and 80 mT. Then, anhysteretic remanent magnetization (ARM) was imparted at a peak AF of 80 mT superimposed on a DC field of 0.1 mT. The ARM was AF demagnetized at the same steps as the AF demagnetization of NRM.

Characteristic remanent magnetization (ChRM) direction was determined using principal component analysis (PCA, Kirschvink 1980; Fig. 4). The demagnetization interval having at least 5 steps with the smallest

Table 1 Results of radiocarbon dating

Dated material (planktonic forams)	Core section	Depth in section [cm]	Depth in core [m]	Measured ^{14}C age [yr bp]	Calendar age [cal yr BP]	
					95% probabry	Median
G. inflata	2	50	0.57	3384±39	3448–3804	3612
G. inflata	3	10	1.17	5338±36	5331–5656	5511
N. dutertrei	3	90	1.97	8460±73	8590–9094	8853
G. inflata	4	20	2.27	9287±48	9676–10,134	9906
N. dutertrei	4	90	2.97	12,233±44	13,409–13,757	13,574
N. dutertrei	5	95	4.02	16,610±53	18,890–19,399	19,138
N. dutertrei	6	60	4.67	18,929±54	21,767–22,250	22,014

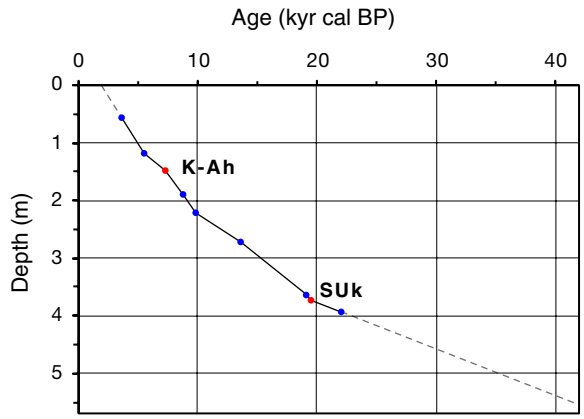

Fig. 3 The age model of Core PC04. Blue dots are based on dating with ^{14}C, and red dots are based on the identification of volcanic ashes: K-Ah: Kikai-Akahoya ash, SUk: Sanbe-Ukinuno ash. The depth scale is the cumulative depth after turbidite and volcanic ash layers were excluded

maximum angular deviation (MAD) was adopted. Samples with MAD > 15° were excluded from further analyses. Samples facing core-section boundaries were also excluded due to potential physical disturbance. RPI was estimated from NRM intensity normalized by ARM. RPI was calculated as a best-fitting slope in a diagram plotting a pair of NRM and ARM for each AF demagnetization step (Channell et al. 2002; Fig. 4). The demagnetization interval having at least 5 steps with the largest correlation coefficient was adopted.

Bulk magnetic properties

Magnetic susceptibility was measured using an AGICO KappaBridge MKF-1 susceptometer at AORI, The University of Tokyo. Magnetic susceptibility represents the concentration of magnetic minerals in sediments. Isothermal remanent magnetization (IRM) was imparted using a pulse magnetizer (Magnetic Measurements MMPM10) and measured using a spinner magnetometer (Natsuhara-Giken SMD-88) at MaCRI, Kochi University. First, IRM was imparted at 2.5 T, which is regarded as saturation IRM (SIRM) in this paper. Then, IRM of 0.3 T were successively imparted in the direction opposite to the initial IRM. S ratio ($S_{-0.3\ T}$) was calculated according to the definition of Bloemendal et al. (1992). $S_{-0.3\ T}$ represents the proportion of magnetic minerals with coercivity lower than 0.3 T, which provides information on magnetic mineralogy in the sediments. ARM before AF demagnetization mentioned above was converted to ARM susceptibility (k_{ARM}), and the ratio of k_{ARM} to SIRM was calculated. k_{ARM} /SIRM is used as a magnetic grain-size proxy (Banarjee et al. 1981; King et al. 1982).

First-order reversal curve (FORC) measurements

FORC diagrams have become widely used in rock- and paleomagnetic studies to characterize quantitatively magnetic mineral assemblages from information on the distribution of coercivity (H_c) and local interaction field (H_u) (Pike et al. 1999; Roberts et al. 2000; 2014; 2022; Egli 2021). We conducted FORC measurements using an alternating-gradient magnetometer (AGM, Princeton Measurements Corporation MicroMag 2900) at AORI, The University of Tokyo. Ten samples were selected from the sediments except for turbidites and volcanic ashes to cover variations of k_{ARM}/SIRM and S ratios. A total of 165 FORCs were measured for each sample, with H_c between 0 and 100 mT, H_u between − 50 and 50 mT, and a field spacing of approximately 1.3 mT. The maximum applied field was 1.0 T, and the averaging time for each measurement point was 200 ms. FORCinel software (Harrison and Feinberg 2008) was used to produce FORC diagrams, and the VARIFORC algorithm of Egli (2013) was used to smooth the data with smoothing parameters of $S_{c0}=4$, $S_{b0}=3$, and $S_{c1}=S_{b1}=7$.

Transmission electron microscopy

We conducted observation of magnetic grains using a transmission electron microscope (TEM) in order to directly observe magnetic grains carrying remanent magnetization, in particular to examine the presence of magnetofossils from the characteristic morphology and grain size confined within the single-domain (SD) range (e.g., Kopp and Kirchvink 2008). Magnetic minerals were extracted from two samples at 1.99 and 5.35 m in depth using a magnetic finger (Kirschvink et al. 1992; Yamazaki and Shimono 2013). A TEM (JEOL JEM-1400) at AORI, The University of Tokyo, operated at 120 kV, was used for the observation.

Grain-size analyses

Grain-size analyses of bulk sediments were conducted using a laser diffraction grain size analyzer (Horiba LA-960) at the National Institute of Advanced Industrial Science and Technology. Twenty-eight samples were selected at approximately the same depth intervals excluding turbidites and volcanic ashes. Small amounts of sediments were taken from the paleomagnetic discrete samples, and they were dispersed well using an ultrasonic bath before the measurement.

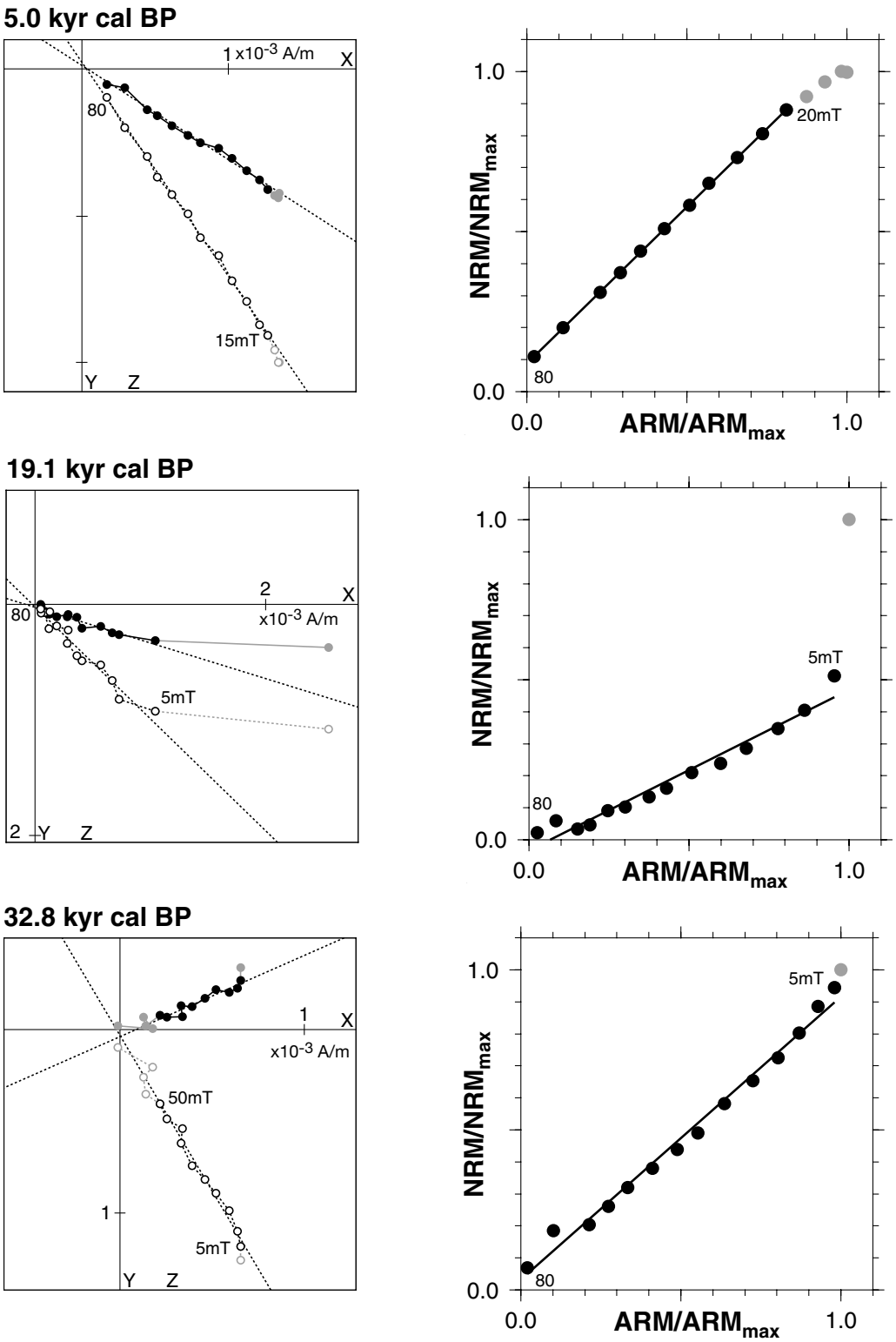

Fig. 4 (Left) Examples of the results of stepwise alternating-field (AF) demagnetization of natural remanent magnetization (NRM). Open (solid) circles are the projection of vector end points on the vertical (horizontal) plane. Numbers attached to the data points are peak AF in mT. Gray data points were not used for calculation of characteristic remanent magnetization directions. The cores are not azimuthally oriented. (Right) Relative paleointensity estimations of corresponding samples from best-fitting slopes on the diagrams plotting a pair of NRM and anhysteretic remanent magnetization (ARM) intensities for each AF demagnetization step. Numbers attached to the data points are peak AF in mT. Gray data points were not used for calculation of best-fitting slopes

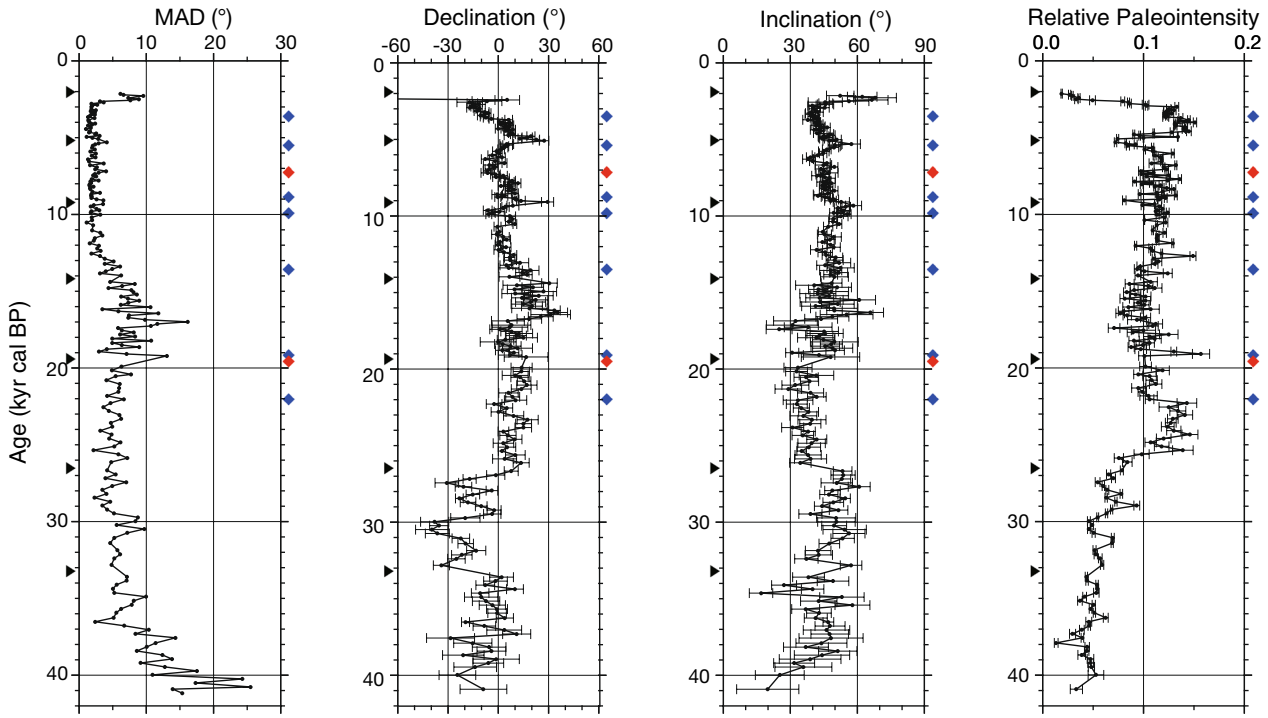

Fig. 5 Maximum angular deviation (MAD), declination, inclination, and relative paleointensity (from left to right) obtained from Core PC04. Blue and red diamonds along the age axis indicate age-control points based on ^{14}C dating and volcanic ashes, respectively. Black triangles show the locations of core-section boundaries. Error bars in declination and inclination are based on MAD values, and those in relative paleointensity are from the uncertainties of the best-fitting slopes in NRM-ARM demagnetization diagrams (Kono and Tanaka 1984)

Results

Paleomagnetic direction and intensity

ChRM directions are well resolved on the Zijderveld diagrams presenting stepwise AF demagnetization of NRM (Fig. 4). MADs of most samples are less than 15° (Fig. 5). A soft secondary component of probably viscous remanent magnetization origin was erased in the first few steps of the AF demagnetization. The PCA fitting was not anchored to the origin, but deviations from the origin were small in general. Figure 5 shows the resultant variations of inclination and declination with age. Declinations are relative because the core was not azimuthally oriented. Here, the mean declination was aligned to zero. Directional variations in the depth scale before excluding turbidites and tephra layers are presented in Additional file 1: Fig. S1. The SUk tephra and some turbidites showed anomalous directions inconsistent with those above and below them.

The directional records of Core PC04 are compared with the records from off Shikoku, Southwest Japan (Ohno et al. 1993) and Lake Biwa, Central Japan (Hayashida et al. 2007) (Fig. 6). All three records show inclinations shallower than that expected from the geocentric axial dipole field at each site. The inclination anomaly around Japan for the last 100 kyr is estimated to be − 2° to − 4° from the global geomagnetic field model for the last 100 kyr (Panovska et al. 2019), which explains only part of the observed shallow inclinations. Hence these inclination records may partly be influenced by inclination shallowing in detrital remanent magnetization (DRM) acquisition processes (e.g., Griffiths et al. 1960). The variation patterns of declination and inclination agree in some time intervals, but there are differences in other intervals. Various factors may be responsible for the differences. The age control of Core PC04 is not good for older than ~ 20 kyr cal BP. In the

(See figure on next page.)

Fig. 6 Comparison of Core PC04 inclination and declination with those of nearby sites: off Shikoku at 32° 09′ N, 133° 54′ E (Ohno et al. 1993) and Lake Biwa at 35° 15′ N, 136° 03′ E (Hayashida et al. 2007). Red lines indicate the horizons of volcanic ashes identified commonly (K-Ah: Kikai-Akahoya ash, SUk: Sanbe-Ukinuno ash, AT: Aira-Tn ash). Red diamonds are the horizons of other ash layers identified only in the Lake Biwa core. Blue lines with GAD: inclinations calculated at individual sites based on the geocentric axial dipole field model. The age models of Ohno et al. (1993) and Hayashida et al. (2007) were recalculated with the methodology used for Core PC04

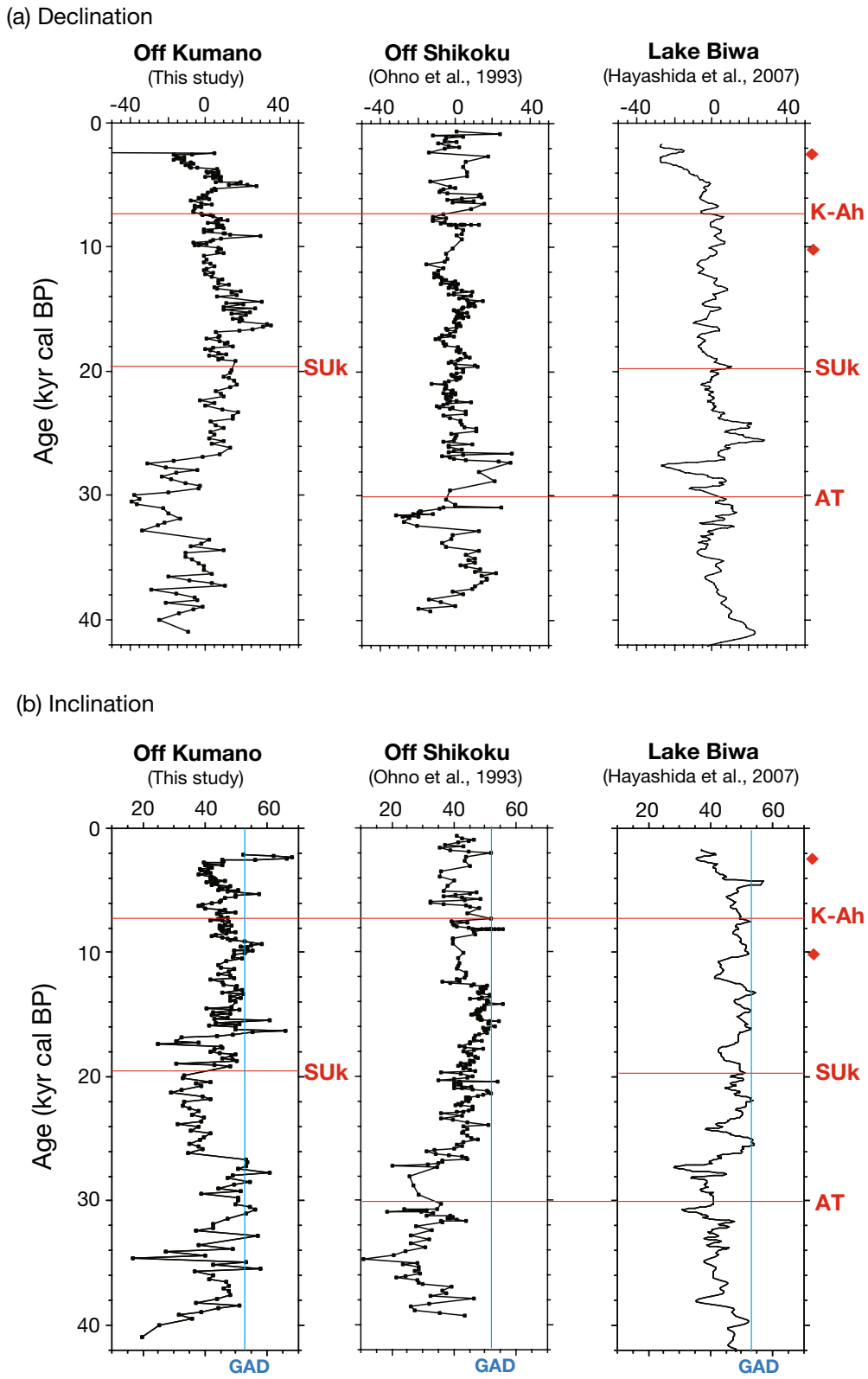

Fig. 6 (See legend on previous page.)

core off Shikoku, turbidite layers might have been overlooked because modern techniques for detecting turbidites such as X-ray CT scan were not available at that time. DRM acquisition processes and lock-in depth in the freshwater sediments of Lake Biwa may be different from those of marine sediments (Tauxe et al. 2006). We consider that the absence of the AT tephra in our core does not necessarily indicate a hiatus. Instead, we infer that the tephra may be diluted by a turbidite and hence not easy to be detected. The horizon expected from the age model corresponds to the interval of frequent thin turbidites.

NRM-ARM demagnetization plots of Core PC04 for calculating RPIs show linear relationship in general except for the first few demagnetization steps (Fig. 4). RPI variations with age are presented in Fig. 5. See Additional file 1: Fig. S1 for RPI in the depth scale including tephras and turbidites. The age of the bottom of the core is estimated to be ~ 40 kyr cal BP, although it is not well constraint. It is inferred that the core does not reach the Laschamp excursion (41.4 ka, Channell et al. 2017) because no directional flip is observed. Alternatively, shallow inclination near the bottom of the core with low RPI might be a manifestation of the Laschamp excursion. Reliability of the obtained RPI record and comparison with other records will be discussed later.

Magnetic and sediment properties

Changes in bulk magnetic properties with age after excluding tephras and turbidites are shown in Fig. 7. See Additional file 1: Fig. S2 for those in the depth scale including tephras and turbidites. Magnetic susceptibility of Core PC04 ranges from ~ 2 to ~ 6×10^{-4} SI excluding tephras and turbidites (Fig. 7a). The two tephras and some turbidites have much higher magnetic susceptibility (Additional file 1: Fig. S2). k_{ARM}/SIRM changes between ~ 1.5 to 5×10^{-4} m/A (Fig. 7c). A lower ratio suggests a larger average magnetic grain size (Banerjee et al. 1981; King et al. 1982). The influence of tephras and turbidites on k_{ARM}/SIRM is small in general, although some of them produce minor peaks or lows (Additional file 1: Fig. S2). This suggests that their magnetic grain sizes do not differ significantly from hemipelagic sediments above and below. Nonetheless, some turbidites accompany anomalously high RPIs (Additional file 1: Fig. S1). $S_{-0.3\ T}$ of 0.95 or higher throughout the core indicates that the magnetization of this core is mainly carried by low-coercivity magnetic minerals like magnetite (Fig. 7d).

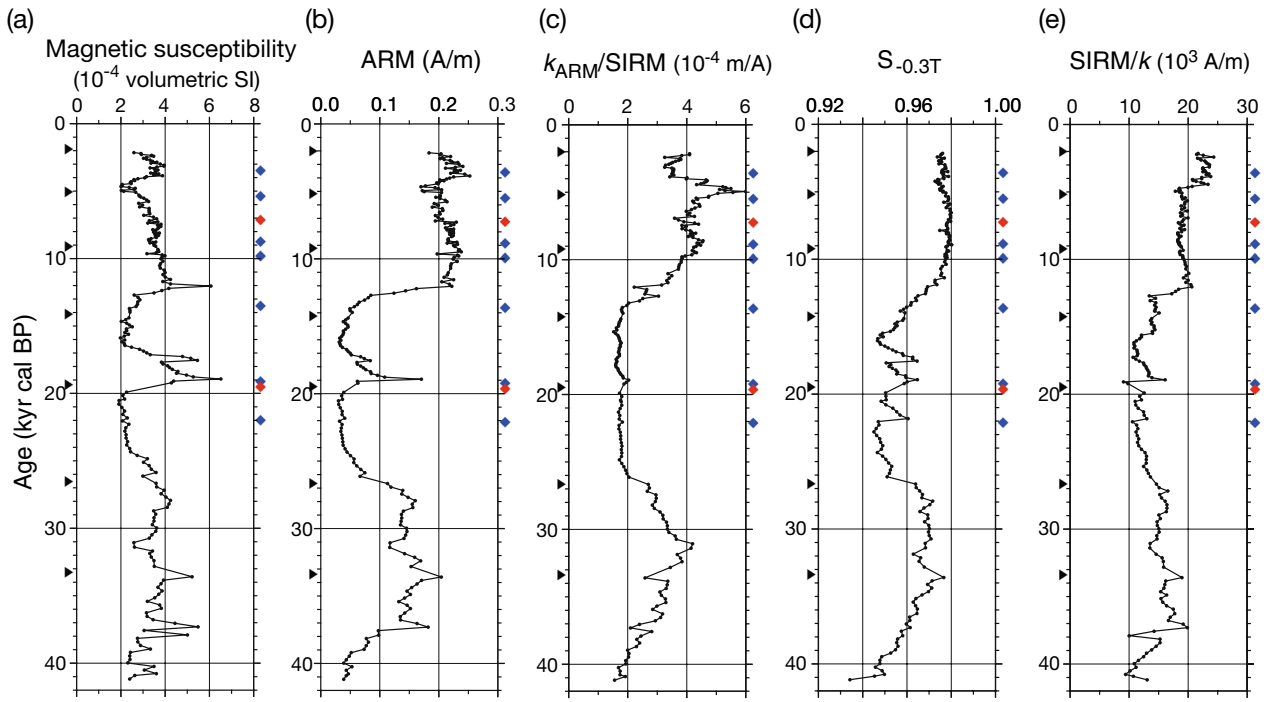

Fig. 7 Bulk magnetic properties of Core PC04. **a** Magnetic susceptibility (k), **b** anhysteretic remanent magnetization (ARM), **c** the ratio of ARM susceptibility (k_{ARM}) to saturation iso-thermal remanent magnetization (SIRM), **d** S ratio ($S_{-0.3\ T}$), and **e** the ratio of SIRM to k. Blue and red diamonds along the age axis indicate age-control points based on ^{14}C dating and volcanic ashes, respectively. Black triangles show the locations of core-section boundaries

These magnetic-property variations indicate that magnetic mineral dissolution by reduction diagenesis has not occurred in the studied sediments. It is well documented that reductive dissolution of magnetic minerals results in one order of magnitude or more drop in magnetic concentration, a coeval increase in average magnetic grain size, and a decrease in $S_{-0.3\ T}$ to ~ 0.8 (Yamazaki et al. 2003; Yamamoto et al. 2007; Korff et al. 2016). The increase in average magnetic grain size is due to earlier loss of finer magnetic grains, and the decrease in $S_{-0.3\ T}$ is due to that high-coercivity magnetic minerals like hematite is more resistive to reduction diagenesis than magnetite. The ratio of SIRM/k less than ~ 25 indicates that greigite formation in anoxic environments has not occurred in the core (Fig. 7e). Sediments containing greigite is known to have high SIRM/k, ~ 30×10^3 A/m or higher (Oldfield et al. 2003; Liu et al. 2018; Chen et al. 2021). In early diagenesis processes, the growth of secondary greigite occurs when reduction further proceeds after magnetite dissolution at a certain depth below the iron-redox boundary (e.g., Roberts 2015). Thus, the absence of greigite estimated from SIRM/k is consistent with the observation that reductive dissolution of magnetite has not started in the studied core.

The magnetic properties presented in Fig. 7 show coeval changes; they are lower between ~ 13 to ~ 27 kyr cal BP except for an increase in magnetic susceptibility between ~ 17 to ~ 20 kyr cal BP. The low k_{ARM}/SIRM and $S_{-0.3\ T}$ indicate that the average magnetic grain size and the proportion of high-coercivity magnetic component are larger in this time interval. The time interval roughly corresponds to the Marine Isotope Stage (MIS) 2, suggesting a connection to global climatic changes. Then, the interval of higher values in the magnetic properties below it might correspond to MIS 3.

The FORC diagrams in the studied sediments show a ridge-like feature along $H_u \approx 0$, which is superimposed on a broad component with a wide H_u distribution (Fig. 8). The former is called the central ridge, which indicates the presence of non-interacting SD grains and is interpreted to be carried by intact chains of magnetofossils (Chen et al. 2007; Yamazaki 2008; Egli et al. 2010; Li Jinhua et al. 2012; Roberts et al. 2012; Chang et al. 2014). The TEM observation supports the existence of magnetofossils (Fig. 9); magnetofossils are identified from the characteristic morphologies, these are hexagonal prism, bullet-shape, and equant octahedron, and SD sizes (tens of nanometers in magnetite). The broad component with a wide H_u distribution indicates the presence of significant magnetostatic interactions, which is interpreted to be carried by interacting SD, vortex, and multi-domain (MD) grains of mainly detrital origin. Magnetofossils of collapsed chains and those originated from magnetotactic bacteria with multistranded magnetosome chains should have significant magnetostatic interactions, and hence also contribute to the broad component. The variations of the FORC distributions among the measured samples are consistent with magnetic grain-size changes estimated from k_{ARM}/SIRM. The peaks in the FORC distributions of samples with lower k_{ARM}/SIRM have lower H_c values around 10 mT, as exemplified by the sample at 17.5 kyr shown in Fig. 8b. The broad component of such samples shows a more MD-like feature; contours of the FORC distributions diverge toward the H_u axis. The extracted central-ridge component is relatively small compared with the ridge-free broad component (Fig. 8d–f). We semi-quantitatively evaluated the proportion of the two components by integrating separately the FORC distributions of the two in the profiles along H_c = 20 mT (Fig. 8g). The result indicates that the FORC proportion of the central-ridge component is about 5% or less, and this does not change significantly within the core. This suggests that the contribution of magnetofossils to the magnetization is minor compared with the detrital component in the studied sediments.

The results of sediment grain-size analyses show that the observed grain-size distribution can be explained by two components assuming a log-normal distribution (Fig. 10a–c); the finer component has the median size of approximately 10 μm, and the median size of the coercer component ranges from ~ 50 to ~ 70 μm. The median size of the former is uniform throughout the core, whereas the size of the latter slightly increases with age (Fig. 10d). The finer component occupies ~ 70% in volume when all grains are assumed to have a spherical shape, and the proportion of the finer component slightly decreases with age (Fig. 10e). Sediment grain-size changes are decoupled from magnetic grain-size variations. Despite the average magnetic grain-size increase between ~ 13 to ~ 27 kyr cal BP, sediment grain size does not show any remarkable change in this time interval.

Discussion

In this study, we have examined magnetic and sedimentological properties of Core PC04 to assess the reliability of the RPI record. Currently, possible influence on RPI of sediment magnetic-property variations associated with environmental changes (so-called "lithological contamination") is a serious problem of RPI estimations (Xuan and Channell 2008; Valet et al. 2011; Yamazaki et al. 2013). Inverse correlation between RPI and k_{ARM}/SIRM is frequently reported in previous RPI studies using marine sediments (Hofmann and Fabian 2009; Sakuramoto et al. 2017; Yamazaki et al. 2013; Inoue et al. 2021; Li Jiaxi et al. 2022). Recent studies indicate that magnetofossils have lower RPI recording efficiency

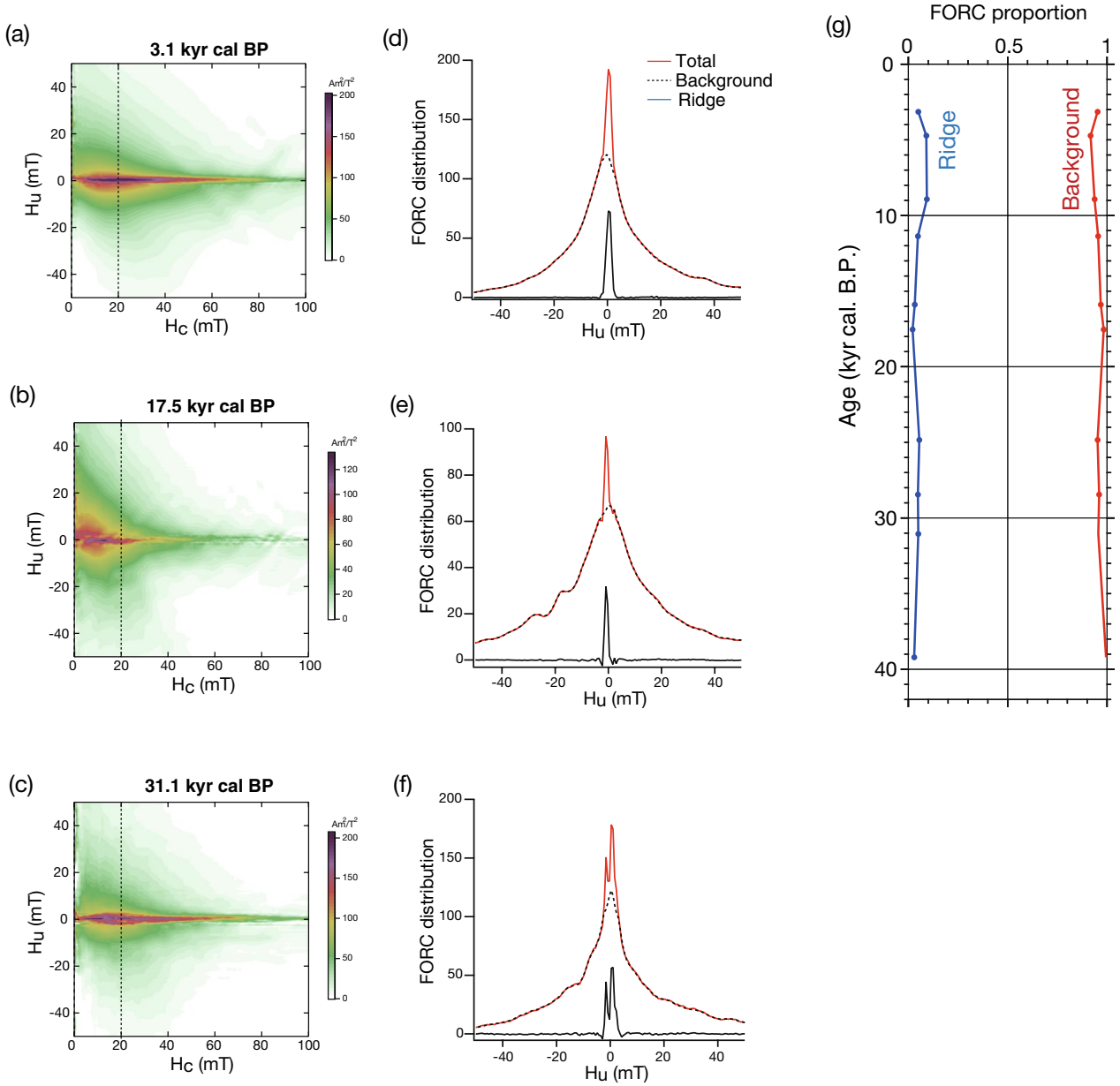

Fig. 8 Results of first-order reversal curve (FORC) measurements. **a**–**c** Examples of FORC diagrams, **d**–**f** profiles of FORC distribution along $H_c = 20$ mT (dashed lines in panels **a**–**c**): the central-ridge component (blue), the ridge-free background component (black), and the total of the two (red), and **g** temporal variations of the relative proportion of the central-ridge component (blue) and the ridge-free background component (red) in FORC distribution based on the integrals of the individual components along $H_c = 20$ mT

than the detrital component (Gai et al. 2021; Inoue et al. 2021; Li Jiaxi et al. 2022; Yamazaki et al. 2023). On the other hand, k_{ARM}/SIRM is a proxy for the proportion of magnetofossils to detrital magnetic minerals (Egli 2004; Yamazaki 2008; Zhang et al. 2022) as well as for magnetic grain size; k_{ARM}/SIRM increases with increasing proportion of magnetofossils. Thus, changing proportion of magnetofossils to detrital magnetic minerals can cause the inverse correlation between RPI and k_{ARM}/SIRM. In the studied core, no correlation between RPI and k_{ARM}/SIRM is observed (Fig. 11a). Our rock-magnetic analyses show that the contribution of magnetofossils to the magnetization of the sediments is very small. It is thus expected that RPI acquisition efficiency of the sediments does not change throughout the core. In this core, k_{ARM}/SIRM is considered to represent magnetic grain-size

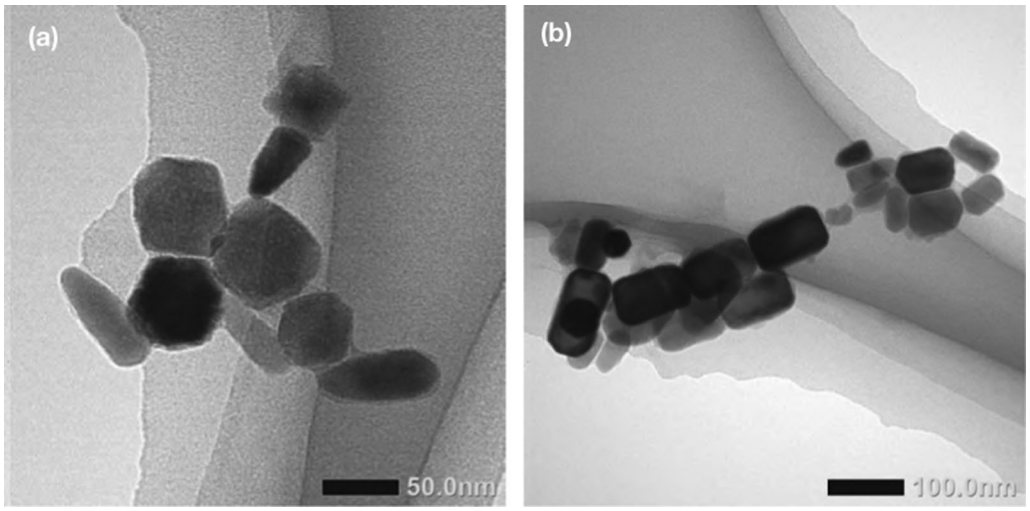

Fig. 9 Transmission electron microscope (TEM) images of magnetofossils extracted from sediments at (a) 8.9 kry cal BP and (b) 28.4 kyr cal BP. scale bar: **a** 50 nm and **b** 100 nm

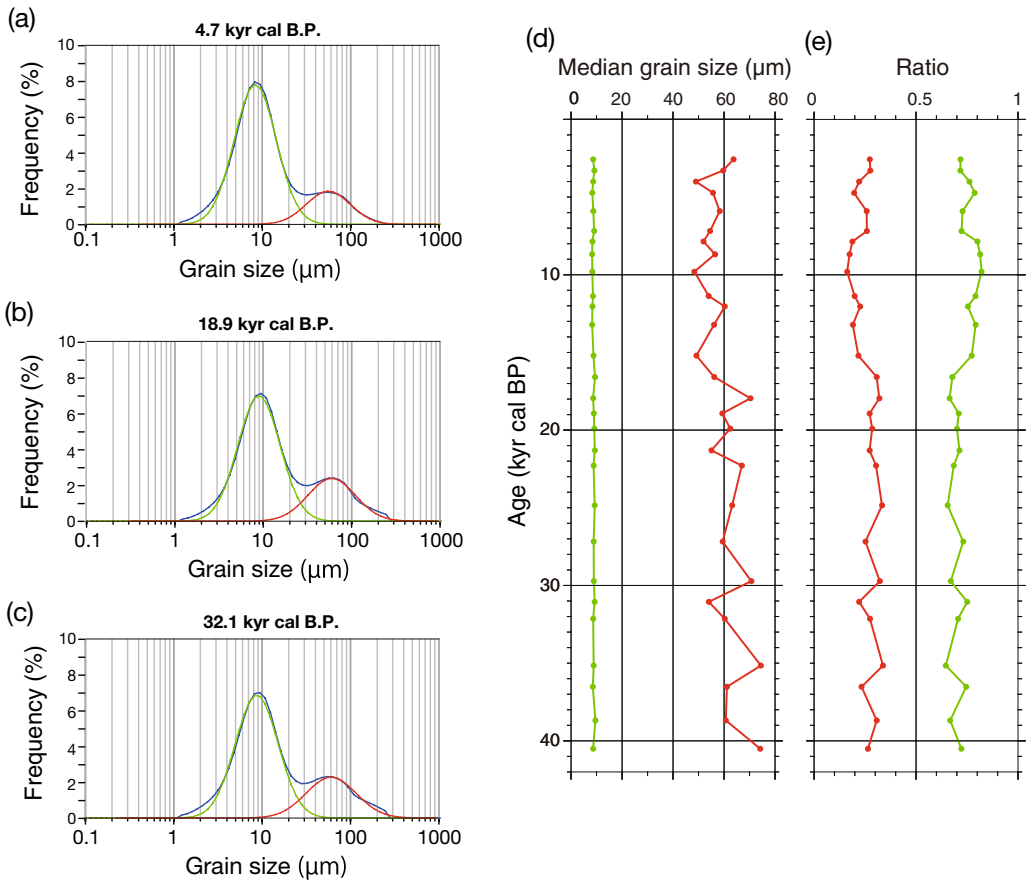

Fig. 10 Results of sediment grain size analyses. **a**–**c** Examples of grain size distribution and fitting with two components assuming log-normal distribution: the coarser (red) and finer (green) components, **d** temporal variations of median grain size of the coarser (red) and finer (green) components, and **e** temporal variations in the volumetric ratio of the coarser (red) and finer (green) components

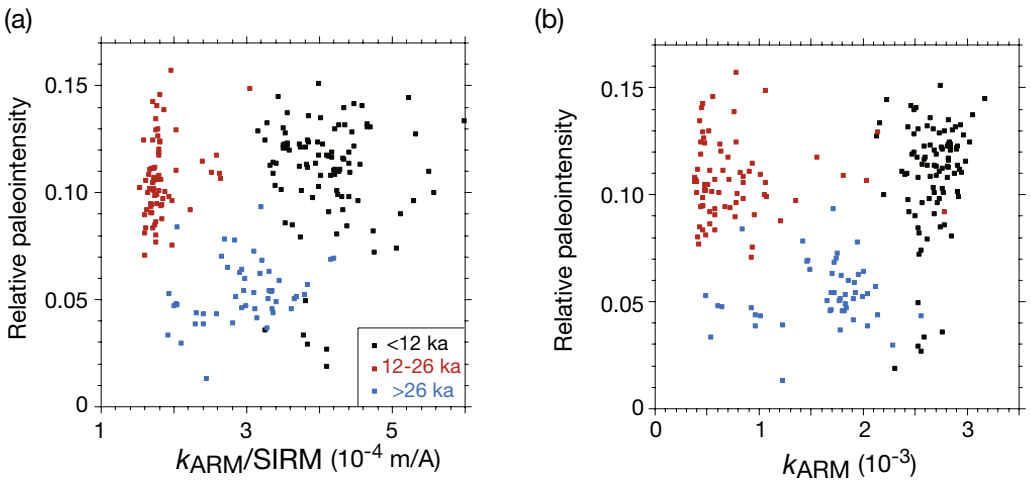

Fig. 11 **a** Relation between relative paleointensity and k_{ARM}/SIRM, and **b** relation between relative paleointensity and k_{ARM}

changes rather than the proportion of magnetofossils to detrital magnetic minerals because of the minor contribution of magnetofossils. In summary, it is considered that the lithological contamination to RPI is minimal in the studied core. In addition, obtained RPIs do not correlate with the normalizer of the RPI estimations, that is ARM, either (Fig. 11b), which also supports the reliability of our RPI record (Tauxe 1993). This implies that differences in the magnetizability of sediments due to the differences in magnetic mineral concentration are appropriately corrected by ARM. In Fig. 11, the data distribution can be divided into three groups, which correspond to different age intervals. k_{ARM}/SIRM and k_{ARM} values younger than ~ 12 ka are high in general, whereas those between ~ 12 to 26 ka are low. They form clusters in Fig. 11 because the upcore transition from low to high are rapid (Fig. 7). The age of the transition roughly corresponds to the MIS 2/1 boundary. The RPI variation ranges in the two age intervals are similar. The low RPI interval older than ~ 26 ka tends to have medium k_{ARM}/SIRM and k_{ARM} values.

In the studied core, there is no sign of magnetic mineral dissolution or secondary greigite formation associated with reduction diagenesis, which may erase and/or overprint original paleomagnetic records. Sediments with high sedimentation rates are preferable for obtaining high-resolution paleomagnetic secular variation records. However, such sediments often have high organic-carbon contents and hence in anoxic environments, where reduction diagenesis prevails (e.g., Yamazaki et al. 2003; Roberts 2015; Korff et al. 2016). It was revealed that sediment grain size is uniform throughout the core when turbidite and volcanic ash layers are excluded. This suggests that hydrodynamic conditions, which may influence DRM acquisition (Jezek and Gilder 2006), would not have changed significantly. Thus, hemipelagic sediments in terminal basins in the Nankai Trough region, which have relatively high sedimentation rates without reduction diagenesis, can

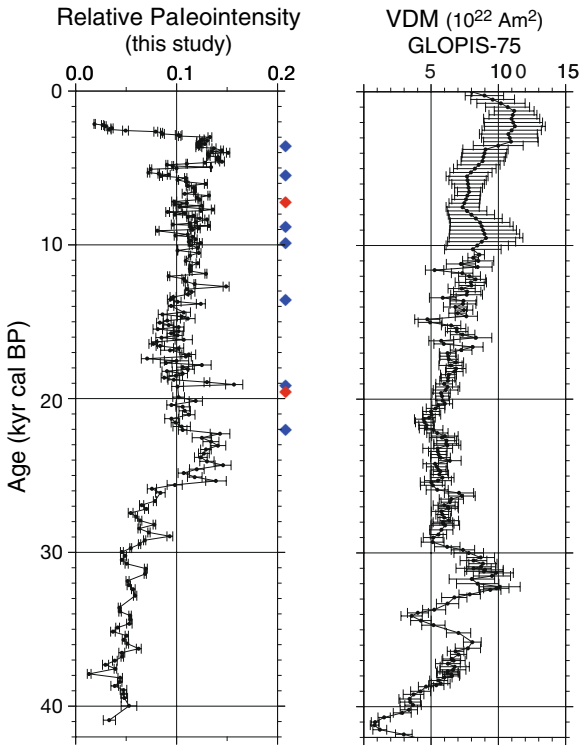

Fig. 12 Comparison of the relative paleointensity record of Core PC04 and the GLOPIS-75 stack (Laj et al. 2014). Blue and red diamonds along the age axis indicate age-control points based on ^{14}C dating and volcanic ashes, respectively

potentially be suitable materials for geomagnetic secular variation studies, although previously they were not used widely. Fluctuations of magnetic mineral concentration, magnetic grain size, and mineralogy in this core are relatively small (Fig. 7), which meets the empirical criteria for reliable RPI estimation (Tauxe 1993).

The RPI record of Core PC04 is compared with the GLOPIS-75 stack covering the last 75 kyr (Laj et al. 2014) (Fig. 12). Both records show an increasing trend since ~ 40 ka. The apparent RPI decease after ~ 3 kyr cal BP in Core PC04 is most likely due to physical disturbance of the very surface sediments at the coring. The RPI increase since the Laschamp Excursion is commonly recognized also in the lower resolution global PRI stacks, Sint-2000 for the last 2 Myr. (Valet et al. 2005) and PISO-1500 for the last 1.5 Myr. (Channell et al. 2009). On the other hand, some shorter time-scale changes do not agree between the two. A high from ~ 25 to ~ 22 kyr cal BP occurs only in Core PC04. However, the PISO-1500 stack also shows a rather strong paleointensity around 22 ka comparable to that during the last 10 ka, although the age resolution is limited. A high from ~ 33 to ~ 30 kyr cal BP exists only in the GLOPIS-75. These differences may suggest existence of a non-dipole field in the Asian region. Alternatively, the GLOPIS-75 stack might be influenced by a non-dipole component; the GLOPIS-75 stack was established by stacking 24 RPI records from the North and South Atlantic Oceans, the Mediterranean, and the Indian Ocean, but the site distribution is still biased in the Atlantic region (Laj et al. 2004). Checking consistency of the PC04 RPI record with other records from nearby sites is hindered by the scarcity of RPI records for the last 40 kyr near Japan except for Holocene. Hayashida et al. (2007) reported normalized intensity, NRM/ARM, from a sediment core in Lake Biwa, Central Japan. Although Hayashida et al. (2007) mentioned that the magnetic properties of the core may not be suitable for RPI reconstruction and avoided to use the term RPI, their record also shows a high between ~ 25 and ~ 22 kyr cal BP when their age model was recalculated using the methodology used for Core PC04.

Further accumulation of reliable regional RPI records with high enough resolution is required to discuss growth and decay of non-dipole components. This study demonstrated that for this purpose hemipelagic sediments with relatively high sedimentation rates deposited in terminal basins between accretionary prisms and forearc basins have potential for recovering high-quality RPI records.

Conclusions

We have presented a RPI record since ~ 40 kyr cal BP obtained from a sediment core taken from the Nankai Trough. RPI in this period was little reported previously from the NE Asian region. Rock magnetic and sediment grain-size analyses revealed that when turbidite and volcanic ash layers are excluded the sediments are homogeneous enough for reliable RPI estimations. Reductive dissolution of magnetic minerals or growth of secondary greigite have not occurred in the studied core. The magnetic minerals in the sediments are mainly of detrital origin, and the contribution of magnetofossils to the magnetization is small. The obtained RPI record shows no sign of lithological contamination. When the RPI record of Core PC04 is compared with that of the GLOPIS-75 stack, an increasing trend since ~ 40 kyr cal BP is commonly observed. On the other hand, there are some differences in shorter timescale variations; a high from ~ 25 to ~ 22 kyr cal BP occurs only in Core PC04, and a high from ~ 33 to ~ 30 kyr cal BP exists only in the GLOPIS-75. Non-dipole fields in the Asian and/or North Atlantic regions may be responsible for the differences.

Abbreviations

AF	Alternating field
AORI	Atmosphere and Ocean Research Institute
ARM	Anhysteretic remanent magnetization
ChRM	Characteristic remanent magnetization
DC	Direct current
DRM	Detrital remanent magnetization
FORC	First-order reversal curve
IRM	Isothermal remanent magnetization
MaCRI	Marine Core Research Institute
MAD	Maximum angular deviation
MD	Multi-domain
NRM	Natural remanent magnetization
PCA	Principal component analysis
RPI	Relative paleointensity
SD	Single domain
SIRM	Saturation IRM
TEM	Transmission electron microscope
XRF	X-ray fluorescence

Supplementary Information

The online version contains supplementary material available at https://doi.org/10.1186/s40623-023-01945-x.

Additional file 1: Fig. S1. Maximum angular deviation (MAD), declination, inclination, and relative paleointensity obtained from Core PC04 in the depth scale before excluding tephra and turbidite layers. **Fig. S2.** Bulk magnetic properties of Core PC04 in the depth scale before excluding tephra and turbidite layers.

Acknowledgements

The core used in this study was obtained by the effort of all personnel related to the R/V Hakuho-maru KH-17-2 cruise. We also thank Yuhji Yamamoto for supporting paleo- and rock magnetic measurements and providing us his software for paleomagnetic data analyses, Yosuke Miyairi and Yusuke Yokoyama for supporting ^{14}C measurements, Futoshi Nanayama for supporting sediment grain-size analysis, and Nobuhiro Ogawa for the help with TEM observation. The manuscript was improved by comments of two anonymous reviewers.

Author contributions
This manuscript is mainly based on RG's work for his Master degree under the supervision of TY, and partly from NO's work for her Ph. D. degree under the supervision of JA. RG and TY wrote the manuscript. All authors contributed interpretation and discussion. All authors read and approved the final manuscript.

Funding
Part of this study was performed under the cooperative research program of Marine Core Research Institute, Kochi University (17A048, 17B048, 19A24, 19B22, 20A008, 20B007), and supported by a Grant-in-Aid for Scientific Research (KAKENHI) of the Japan Society for the Promotion of Science (19H01997 and 21H01171).

Availability of data and materials
The paleo- and rock magnetic data produced in this study are available in Zenodo repository at https://doi.org/https://doi.org/10.5281/zenodo.8317478.

Declarations

Competing interests
The authors declare that they have no competing interests.

Author details
[1]Atmosphere and Ocean Research Institute, The University of Tokyo, Kashiwa, Japan. [2]Ministry of Education, Culture, Sports, Science and Technology, Tokyo, Japan. [3]Institute for Marine-Earth Exploration and Engineering, Japan Agency for Marine-Earth Science and Technology, Yokosuka, Japan.

Received: 8 September 2023 Accepted: 9 December 2023
Published online: 03 January 2024

References

Albert PG, Smith VC, Suzuki T, Tomlinson EL, Nakagawa T, McLean D, Yamada M, Staff RA, Schlolaut G, Takemura K, Nagahashi Y, Kimura J-I, Suigetsu 2006 Project Members (2018) Constraints on the frequency and dispersal of explosive eruptions at Sambe and Daisen volcanoes (South-West Japan Arc) from the distal Lake Suigetsu record (SG06 core). Earth-Sci Rev 185:1004–1028. https://doi.org/10.1016/j.earscirev.2018.07.003

Albert PG, Smith VC, Suzuki T, McLean D, Tomlinson EL, Miyabuchi Y, Kitaba I, Mark DF, Moriwaki M, Nakagawa T, Suigetsu 2006 Project Members (2019) Geochemical characterisation of the Late Quaternary widespread Japanese tephrostratigraphic markers and correlations to the Lake Suigetsu sedimentary archive (SG06 core). Quat Geochronol 52:103–131. https://doi.org/10.1016/j.quageo.2019.01.005

Banerjee SK, King J, Marvin J (1981) A rapid method for magnetic granulometry with applications to environmental studies. Geophys Res Lett 8:333–336

Bloemendal J, King JW, Hall FR, Doh SJ (1992) Rock magnetism of late Neogene and Pleistocene deep-sea sediments: relationship to sediment source, diagenetic processes, and sediment lithology. J Geophys Res 97:4361–4375. https://doi.org/10.1029/91JB0306

Bronk Ramsey C (2009) Bayesian analysis of radiocarbon dates. Radiocarbon 51:337–360

Chang L, Roberts AP, Winklhofer M, Heslop D, Dekkers MJ, Krijgsman W, Fitz Gerald JD, Smith P (2014) Magnetic detection and characterization of biogenic magnetic minerals: a comparison of ferromagnetic resonance and first-order reversal curve diagrams. J Geophys Res: Solid Earth 119:6136–6158. https://doi.org/10.1002/2014JB011213

Channell JET, Mazaud A, Sullivan P, Turner S, Raymo ME (2002) Geomagnetic excursions and paleointensities in the Matuyama Chron at Ocean Drilling Program Sites 983 and 984 (Iceland Basin). J Geophys Res 107:2114. https://doi.org/10.1029/2001JB000491

Channell JET, Xuan C, Hodell DA (2009) Stacking paleointensity and oxygen isotope data for the last 1.5 Myr (PISO-1500). Earth Planet Sci Lett 283:14–23. https://doi.org/10.1016/J.EPSL.2009.03.012

Channell JET, Vázquez Riveiroset N, Gottschalk J, Waelbroeck C, Skinner LC (2017) Age and duration of Laschamp and Iceland Basin geomagnetic excursions in the South Atlantic Ocean. Quat Sci Rev 167:1–13. https://doi.org/10.1016/j.quascirev.2017.04.020

Chen AP, Egli R, Moskowitz BM (2007) First-order reversal curve (FORC) diagrams of natural and cultured biogenic magnetic particles. J Geophys Res 112:B08S90. https://doi.org/10.1029/2006jb004575

Chen Y, Zhang W, Nian X, Sun Q, Ge C, Hutchinson SM, Cheng Q, Wang F, Chen J, Zhao X (2021) Greigite as an indicator for salinity and sedimentation rate change: evidence from the Yangtze river delta, China. J Geophys Res: Sold Earth 126. https://doi.org/10.1029/2020JB021085

Egli R (2004) Characterization of individual rock magnetic components by analysis of remanence curves: 2. Fundamental properties of coercivity distributions. Phys Chem Earth 29:851–867. https://doi.org/10.1016/J.PCE.2004.04.001

Egli R (2013) VARIFORC: An optimized protocol for calculating non-regular first-order reversal curve (FORC) diagrams. Glob Planet Change 110:302–320. https://doi.org/10.1016/j.gloplacha.2013.08.003

Egli R (2021) Magnetic characterization of geologic materials with first-order reversal curves. In: Franco V, Dodrill B (eds) Magnetic measurement techniques for materials characterization. Springer, Berlin, pp 455–604. https://doi.org/10.1007/978-3-030-70443-8_17

Egli R, Chen AP, Winklhofer M, Kodama KP, Horng CS (2010) Detection of noninteracting single domain particles using first-order reversal curve diagrams. Geochem Geophys Geosyst 11:Q01Z11. https://doi.org/10.1029/2009gc002916

Gai C, Liu Y, Shi X, Sun C, Jiang X, Liu J, Zhong Y, Liu Q (2021) Recording fidelity of relative paleointensity characteristics in the North Pacific Ocean. J Geophys Res: Solid Earth 126. https://doi.org/10.1029/2021JB022068

Griffiths DH, King RF, Rees AI, Wright AE (1960) The remanent magnetism of some recent varved sediments. Proc R Soc A 256:359–383. https://doi.org/10.1098/rspa.1960.0113

Harrison RJ, Feinberg JM (2008) FORCinel: an improved algorithm for calculating first-order reversal curve distributions using locally weighted regression smoothing. Geochem Geophys Geosyst 9:Q05016. https://doi.org/10.1029/2008GC001987

Hayashida A, Ali M, Kuniko Y, Kitagawa H, Torii M, Takemura K (2007) Environmental magnetic record and paleosecular variation data for the last 40 kyrs from the Lake Biwa sediments, Central Japan. Earth Planets Space 59:807–814. https://doi.org/10.1186/BF03352743

Heaton TJ, Köhler P, Butzin M, Bard E, Reimer RW, Austin WE, Bronk Ramsey C, Grootes MP, Hughen AK, Kromer B, Reimer JP, Adkins J, Burke A, Cook SM, Olsen J, Skinner CL (2020) Marine20—the marine radiocarbon age calibration curve (0–55,000 cal BP). Radiocarbon 62:779–820. https://doi.org/10.1017/RDC.2020.68

Hofmann DI, Fabian K (2009) Correcting relative paleointensity records for variations in sediment composition: results from a South Atlantic stratigraphic network. Earth Planet Sci Lett 284:34–43. https://doi.org/10.1016/j.epsl.2009.03.043

Hsiung K-H, Kanamatsu T, Ikehara K, Usami K, Horng C-S, Ohkouchi N, Ogawa NO, Saito S, Murayama M (2021) X-ray fluorescence core scanning, magnetic signatures, and organic geochemistry analyses of Ryukyu Trench sediments: turbidites and hemipelagites. Prog Earth Planet Sci 8:2. https://doi.org/10.1186/s40645-020-00396-2

Inoue K, Yamazaki T, Usui Y (2021) Influence of magnetofossils on paleointensity estimations inferred from principal component analyses of first-order reversal curve diagrams for sediments from the western equatorial Pacific. Geochem Geophys Geosyst 22. https://doi.org/10.1029/2021GC010081

Jezek J, Gilder SA (2006) Competition of magnetic and hydrodynamic forces on ellipsoidal particles under shear: influence of the Earth's magnetic field on particle alignment in viscous media. J Geophys Res 111:B12S23. https://doi.org/10.1029/2006JB004541

Li Jiaxi, Yamazaki T, Usui Y, Sagawa T, Kubota Y, Kuroda J (2022) Understanding the role of biogenic magnetite in geomagnetic paleointensity recording: insights from Ontong Java Plateau sediments. J Geophys Res: Solid Earth 127. https://doi.org/10.1029/2022JB024387

Jinhua Li, Wu W, Liu Q, Pan Y (2012) Magnetic anisotropy, magnetostatic interactions and identification of magnetofossils. Geochem Geophys Geosyst 13:Q10Z51. https://doi.org/10.1029/2012GC004384

Kanamatsu T, Usami K, McHugh CM, Ikehara K (2017) High-resolution chronology of sediment below CCD based on Holocene paleomagnetic secular variations in the Tohoku-oki earthquake rupture zone.

Geochem Geophys Geosyst 18:2990–3002. https://doi.org/10.1002/2017GC006878
King J, Banerjee SK, Marvin J, Özdemir Ö (1982) A comparison of different magnetic methods for determining the relative grain size of magnetite in natural materials: some results from lake sediments. Earth Planet Sci Lett 59:404–419. https://doi.org/10.1016/0012-821X(82)90142-X
Kirschvink JL (1980) The least-squares line and plane and the analysis of palaeomagnetic data. Geophys J R Astron Soc 62:699–718. https://doi.org/10.1111/j.1365-246X.1980.tb02601.x
Kirschvink JL, Kobayashi-Kirschvink A, Woodford BJ (1992) Magnetite biomineralization in the human brain. Proc Natl Acad Sci USA 89:7683–7687
Kono M, Tanaka H (1984) Analysis of the Thellier's method of paleointensity determination 1: estimation of statistical error. J Geomag Geoelectr 36:267–284
Kopp RE, Kirschvink JL (2008) The identification and biogeochemical interpretation of fossil magnetotactic bacteria. Earth-Sci Rev 86:42–61. https://doi.org/10.1016/J.EARSCIREV.2007.08.001
Korff L, von Dobeneck T, Frederichs T, Kasten S, Kuhn G, Gersonde R, Diekmann B (2016) Cyclic magnetite dissolution in Pleistocene sediments of the abyssal northwest Pacific Ocean: evidence for glacial oxygen depletion and carbon trapping. Paleoceanography 31:600–624. https://doi.org/10.1002/2015PA002882
Korte M, Constable C, Donadini F, Holme R (2011) Reconstructing the Holocene geomagnetic field. Earth Planet Sci Lett 312:497–505
Korte M, Brown MC, Gunnarson SR, Nilsson A, Panovska S, Wardinski I, Constable CG (2019) Refining Holocene geochronologies using palaeomagnetic records. Quat Geochronol 50:47–74. https://doi.org/10.1016/j.quageo.2018.11.004
Laj C, Guillou H, Kissel C (2014) Dynamics of the earth magnetic field in the 10–75 kyr period comprising the Laschamp and Mono Lake excursions: new results from the French Chaîne des Puys in a global perspective. Earth Planet Sci Lett 387:184–197. https://doi.org/10.1016/j.epsl.2013.11.031
Laj C, Kissel C, Beer J. (2004) High resolution global paleointensity stack since 75 kyr (GLOPIS-75) calibrated to absolute values. In: Timescales of the geomagnetic field, AGU Monogr 145:255–265
Liu J, Mei X, Shi X, Liu Q, Liu Y, Ge S (2018) Formation and preservation of greigite (Fe_3S_4) in a thick sediment layer from the central South Yellow Sea. Geophys J Int 213:135–146
Merrill RT, McElhinny MW, McFadden PL (1998) The magnetic field of the earth. Academic Press, San Diego
Ohno M, Hamano Y, Murayama M, Matsumoto E, Iwakura H, Nakamura T, Taira A (1993) Paleomagnetic record over the past 35,000 years of a sediment core from off Shikoku, southwest Japan. Geophys Res Lett 20:1395–1398. https://doi.org/10.1029/93GL01241
Okutsu N, Ashi J, Yamaguchi A, Irino T, Ikehara K, Kanamatsu T, Suganuma Y, Maruyama M (2018) Evidence for surface sediment remobilization by earthquakes in the Nankai forearc region from sedimentary records. In: Lintern DG, Mosher DC, Moscardelli LG, Bobrowsky PT, Campbell C, Chaytor JD, Clague JJ, Georgiopoulou A, Lajeunesse P, Normandeau AA, Piper DJW, Scherwath M, Stacey C, Turmel D (eds) Subaqueous mass movements. Geol Soc Lond Spec Publ 477:37–45. https://doi.org/10.1144/SP477.22
Okutsu N (2019) A fundamental research of fine-grained turbidites for reconstructing the seismic history in the Nankai Trough. PhD Dissertation, The University of Tokyo
Oldfield F, Wake R, Boyle J, Jones R, Nolan S, Gibbs Z, Appleby P, Fisher E, Wolff G (2003) The late-Holocene history of Gormire Lake (NE England) and its catchment: a multiproxy reconstruction of past human impact. Holocene 13:677–690. https://doi.org/10.1191/0959683603hl654rp
Panovska S, Constable CG, Korte M (2018) Extending global continuous geomagnetic field reconstructions on timescales beyond human civilization. Geochem Geophys Geosyst 19:4757–4772. https://doi.org/10.1029/2018GC007966
Panovska S, Korte M, Constable CG (2019) One hundred thousand years of geomagnetic field evolution. Rev Geophys 57:1289–1337. https://doi.org/10.1029/2019RG000656
Pike CR, Roberts AP, Verosub KL (1999) Characterizing interactions in fine magnetic particle systems using first order reversal curves. J Appl Phys 85:6660–6667. https://doi.org/10.1063/1.370176
Roberts AP (2015) Magnetic mineral diagenesis. Earth-Sci Rev 151:1–47. https://doi.org/10.1016/j.earscirev.2015.09.010
Roberts AP, Pike CR, Verosub KL (2000) First-order reversal curve diagrams: a new tool for characterizing the magnetic properties of natural samples. J Geophys Res 105:28461–28475. https://doi.org/10.1029/2000jb900326
Roberts AP, Chang L, Heslop D, Florindo F, Larrasoaña JC (2012) Searching for single domain magnetite in the "pseudo-single- domain" sedimentary haystack: implications of biogenic magnetite preservation for sediment magnetism and relative paleointensity determinations. J Geophys Res: Solid Earth 117:B08104. https://doi.org/10.1029/2012JB009412
Roberts AP, Heslop D, Zhao X, Pike CR (2014) Understanding fine magnetic particle systems through use of first-order reversal curve diagrams. Rev Geophys 52:557–602. https://doi.org/10.1002/2014RG000462
Roberts AP, Heslop D, Zhao X, Oda H, Egli R, Harrison RJ, Hu P, Muxworthy AR, Sato T (2022) Unlocking information about fine magnetic particle assemblages from first-order reversal curve diagrams: recent advances. Earth-Sci Rev 227. https://doi.org/10.1016/j.earscirev.2022.103950
Rothwell RG, Hoogakker B, Thomson J, Croudace IW, Frenz M (2006) Turbidite emplacement on the southern Balearic Abyssal Plain (western Mediterranean Sea) during Marine Isotope Stages 1-3: an application of ITRAX XRF scanning of sediment cores to lithostratigraphic analysis. In: New techniques in sediment core analysis, Geol Soc Lond Spec Publ 267:79–98
Sakuramoto Y, Yamazaki T, Kimoto K, Miyairi Y, Kuroda J, Yokoyama Y, Matsuzaki H (2017) A geomagnetic paleointensity record of 0.6 to 3.2 Ma from sediments in the western equatorial Pacific and remanent magnetization lock-in depth. J Geophys Res: Solid Earth 122:7525–7543. https://doi.org/10.1002/2017JB014450
Tauxe L (1993) Sedimentary records of relative paleointensity of the geomagnetic field: theory and practice. Rev Geophys 31:319–354. https://doi.org/10.1029/93RG01771
Tauxe L, Steindorf JL, Harris A (2006) Depositional remanent magnetization: toward an improved theoretical and experimental foundation. Earth Planet Sci Lett 244:515–529
Valet J-P, Meynadier L, Guyodo Y (2005) Geomagnetic dipole strength and reversal rate over the past two million years. Nature 435:802–805. https://doi.org/10.1038/nature03674
Valet J-P, Moreno E, Bassinot F, Johannes L, Dewilde F, Bastos T, Lefort A, Vence-Peyre M-T (2011) Isolating climatic and paleomagnetic imbricated signals in two marine cores using principal component analysis. Geochem Geophys Geosyst 12:Q08012. https://doi.org/10.1029/2011GC003697
Van Daele M, Cnudde V, Duyck P, Pino M, Urrutia R, De Batist M (2014) Multidirectional, synchronously-triggered seismo-turbidites and debrites revealed by X-ray computed tomography (CT). Sedimentology 61:861–880. https://doi.org/10.1111/sed.12070
Xuan C, Channell JET (2008) Origin of orbital periods in the sedimentary relative paleointensity records. Phys Earth Planet Int 169:140–151. https://doi.org/10.1016/j.pepi.2008.07.017
Yamamoto Y, Yamazaki T, Kanamatsu T, Ioka N, Mishima T (2007) Relative paleointensity stack during the last 250 kyr in the northwest Pacific. J Geophys Res 112:B01104. https://doi.org/10.1029/2006JB004477
Yamazaki T (2008) Magnetostatic interactions in deep-sea sediments inferred from first-order reversal curve diagrams: implications for relative paleointensity normalization. Geochem Geophys Geosyst 9:Q02005. https://doi.org/10.1029/2007GC001797
Yamazaki T, Shimono T (2013) Abundant bacterial magnetite occurrence in oxic red clay. Geology 41:1191–1194. https://doi.org/10.1130/G34782.1
Yamazaki T, Abdeldayem AL, Ikehara K (2003) Rock-magnetic changes with reduction diagenesis in Japan Sea sediments and preservation of geomagnetic secular variation in inclination during the last 30,000 years. Earth Planets Space 55:327–340. https://doi.org/10.1186/BF03351766
Yamazaki T, Yamamoto Y, Acton G, Guidry EP, Richter C (2013) Rock-magnetic artifacts on long-term relative paleointensity variations in sediments. Geochem Geophys Geosyst 14:29–43. https://doi.org/10.1002/ggge.20064
Yamazaki T, Li J, Shimono T, Kanamatsu T (2023) Difference in relative paleointensity recording efficiency of magnetic mineral constituents in a

sediment core off Chile. J Geophys Res: Solid Earth 128. https://doi.org/10.1029/2023JB026816
Zhang Q, Roberts AP, Ge S, Liu Y, Liu J, Liu S, Tang X, Wang H, Wang D, Li J, Liu Q (2022) Interpretation of anhysteretic remanent magnetization carriers in magnetofossil-rich marine sediments. J Geophys Res: Solid Earth 127. https://doi.org/10.1029/2022JB024432

Publisher's Note